Turning manganese into gold: Efficient electrochemical CO2 reduction by a fac-Mn(apbpy)(CO)3Br complex in a gas–liquid interface flow cell

Turning Manganese into Gold: efficient electrochemical CO_2 reduction by a *fac*-Mn(apbpy)$(CO)_3$Br complex in a gas-liquid interface flow cell

Jonathan Filippi,[a] Laura Rotundo,[b] Roberto Gobetto,[*b] Hamish A. Miller,[a] Carlo Nervi,[*b] Alessandro Lavacchi,[a] Francesco Vizza[*a]

a. ICCOM-CNR, via Madonna del Piano 10, 50019 Sesto Fiorentino (FI), Italy. E-mail: francesco.vizza@iccom.cnr.it

b. Department of Chemistry and NIS (Centre of excellence), University of Torino via P. Giuria 7, 10125 Torino, Italy. E-mail: carlo.nervi@unito.it

Abstract: The electrochemical reduction of carbon dioxide (CO_2RR) is a viable route for the transformation of intermittent renewable energy into high energy density chemical vectors (e.g. CO) or into fuels. Unlike metal nanoparticle electrocatalysts, the use of organometallic molecular complexes affords more efficient metal utilization, limits poisoning phenomena and allows the tuning of selectivity by varying the electronic and coordination properties of the metal center. Herein we describe the organometallic complex (*fac*-Mn(apbpy)$(CO)_3$Br) (apbpy = 4-(4-aminophenyl)-2,2'-bipyridine) covalently anchored on a gas diffusion layer used as cathode in an aqueous gas-liquid interface complete electrolysis flow cell microreactor. The decorated gas diffusion layer electrode was able to convert CO_2 into CO and HCOOH with faradaic efficiencies (FE) of 76% and 10% with a CO-productivity close to 70 Nl min^{-1} g_{Mn}^{-1} reaching CO_2RR turnover numbers up to $1.6 \cdot 10^5$ largely outperforming a state-of-the-art gold nanoparticle electrocatalyst (Au/C 10 wt%) operating in the same cell conditions.

1 Introduction:

The CO_2 concentration in the atmosphere caused by anthropogenic activities, strongly connected to the conversion of fossil fuels into energy, is an exponential increasing concern because it causes environmental issues, such as flooding and dramatic weather events. The energy demand of our society is constantly increasing, and the CO_2 environmental and energy problems are strictly related. Thus, a green, fast and economic chemical way to convert CO_2 back into fuels is highly desirable. To be feasible the process should be also economically sustainable, for example coupling the CO_2 capture with rare earth recycling or CO_2 conversion to CO with direct utilization for pharmaceutical high-value products[1,2]. Carbon dioxide electro-reduction (CO_2RR), represents an excellent candidate for recycling CO_2 back into high density energy vectors (fuels), and chemicals by exploiting excess electrical energy produced by discontinuous and intermittent renewable energy sources. Generally, the CO_2 electrolysis process can produce a plethora of products such as CO, CH_4, C_2H_4, formate, methanol and ethanol depending on the nature of the electrocatalyst and on reaction conditions, such as electrode potential, electrolyte, pressure and temperature [3-14]. Syngas (CO/H_2 mixtures) produced by simultaneous CO_2RR and water reduction can be considered a good candidate, being a potential building block for larger molecules (using gas-to-liquid processes such as Fischer-Tropsch) [12,13]. When targeting CO_2 reduction products (CO, CH_4, C_2H_4 alcohols, etc.) in aqueous media, CO_2RR is limited by parasitic water reduction, lowering the quantity of charge that effectively is used to convert CO_2, hence, reducing the energy efficiency of the whole process [11,14].

Electrocatalytic structures based on metal nanoparticles are known to convert CO_2 to CO: gold, silver, palladium and, to a certain extent, copper are able to produce CO under a variety of conditions, including in aqueous media [11,13-20]. The use of metal based catalysts usually requires high metal loadings and careful nanoparticle morphology control in order to guarantee selectivity and faradaic efficiencies and avoid performance degradation due to nanoparticle

coalescence phenomena. The use of organometallic molecular complexes as electrocatalysts for CO_2 electroreduction is a viable strategy to overcome such limitations affording more efficient metal utilization (as it is intrinsically single site) and allowing the possibility to control the selectivity and the activity of the electrocatalyst by adjusting the coordination of the metal center to tune both electronic properties and steric hindrance [21-28]. Furthermore, the immobilization of organometallic complexes on a conductive support has been proven to be an extremely powerful tool to further improve the advantages of the use of organometallic complexes [29-47]. In particular when covalently bound, resulting in faster electron transfer kinetics, higher TOFs and TONs, and significant improved stability when compared to the same catalyst dissolved in solution [45-47]. In our previous work we described the use of a *fac*-Mn(apbpy)$(CO)_3$Br complex grafted electrochemically onto a carbon cloth support via electrochemical diazonium salt reduction (figure S1). The electrode, immersed in a CO_2-saturated aqueous $KHCO_3$ solution, was able to convert selectively CO_2 into CO at 60% faradaic efficiency (FE) at -0.716 V vs RHE together with a productivity rate higher than 14.5 Nl_{CO} min^{-1} g_{Mn}^{-1} with turnover numbers of up to 33200 during 10 hours of operation [47]. In order to effectively establish an optimized three-phase boundary between water (necessary as proton source), electrocatalyst and CO_2 gas we chose a buffer layer configuration (figure 1) to ensure proper hydration of the electrocatalytic layer [49-53]. Furthermore, hydration also controls the local pH at the electrocatalyst interface, that also influences the selectivity between different CO_2RR products [54-64].

Herein, we describe the performance of a complete CO_2RR electrolyzer employing a single-site manganese-based molecular electrocatalyst for efficient and selective conversion of CO_2 to CO (and HCOOH) in aqueous media with high faradaic selectivity, metal efficiency and turnover numbers. This system is the first example of a covalently grafted molecular complex employed in a complete electrolyzer.

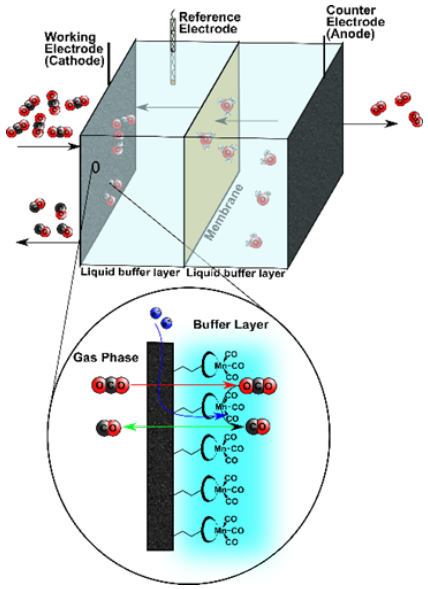

Figure 1: Gas diffusion layer-supported *fac*-Mn(apbpy)$(CO)_3$Br electrocatalyst at the interface between gas and buffer layer phase in the flow electrochemical cell

2 Methods:

2.1 Synthesis of the electrocatalysts

2.1.1 Synthesis of the *fac*-Mn(apbpy)$(CO)_3$Br complex

The complex *fac*-Mn(apbpy)$(CO)_3$Br was synthesized reacting 4-(4-aminophenyl)-2,2'-bipyridine (apbpy) with the corresponding precursor $Mn(CO)_5Br$, following a similar synthetic approach as previously reported [46,47].

2.1.2 Molecular cathode preparation on carbon cloth

The molecular complex fac-Mn(apbpy)$(CO)_3$Br was supported on carbon cloth gas diffusion layer by electrochemical diazonium salt reduction (scheme S1). First the pristine carbon cloth GDL (GPP050M from Cetech Co. ltd) was cut in pieces of 37 x 30 mm and cleaned ultrasonically in 50 wt% 2-propanol solution in Milliq water for 30' and in pure Milliq water for additional 30', then dried in an oven at 60°C for one hour. The real electrochemical surface area (ECSA) was estimated

by performing cyclic voltammetry on a 1.0 mM solution of ferrocene (Fc) at different scan rates (the diffusion coefficient of Fc is $2.24 \cdot 10^{-5}$ cm^2 s^{-1}). The peak current was then plotted against the square of the scan rate and the slope is used to determine the real surface area according to the Randles-Sevčik law. The estimated roughness factor (fr = AECSA / AGEOM) was 5.87, as it has been previously reported by us [47]. The fac-Mn(apbpy)$(CO)_3$Br diazonium salt was synthesized directly into the preparative electrochemical cell under inert atmosphere from a solution of the corresponding complex ($5 \cdot 10^{-3}$ M) and 30 µl of trichloroacetic acid (Sigma) in 10 ml of acetonitrile (Sigma). The solution was initially cooled in an ice water bath, then 10 µl of isoamyl nitrite and TBAPF6 (0.1M) were added. The carbon cloth functionalization was executed by performing cyclic voltammetry scans between +0.65 and -0.7 V (vs Ag|AgCl|KCl_{sat}) at 0.05 V s^{-1} in cathodic direction as previously described [47].

2.1.3 Molecular cathode loading estimation:

For quantification of the amount of electrocatalyst covalently bonded on ECSA, the electrochemical method of charge integration of CV scan could be adopted [46,65]. However, the electrochemical reduction of the *fac*-Mn(apbpy)$(CO)_3$Br/CC is chemically irreversible (as it is in homogenous conditions) and overlaps with the reduction of water. An indirect method for evaluating the surface coverage Γ (mol cm^{-2}) is via charge integration of CV data of CC bonded nitroaniline. This approach has the advantage of using an electrochemically reversible system in MeCN solutions, and it has Γ values about 10 times higher than those of bpy-type metal complexes, as previously reported [46,65]. The surface coverage of nitroaniline on CC has been experimentally evaluated to be 1.4 10^{-8} mol cm_{ECSA}^{-2} [47]. This value is comparable with that previously found for glassy carbon electrode (about 10^{-9} mol cm^{-2}), considering the much higher roughness of CC. Hence, the estimated electrocatalyst surface loading from CV charge integration was $1.4 \cdot 10^{-9}$ mol cm_{ECSA}^{-2} ($4.51 \cdot 10^{-7}$ g_{Mn} cm_{geom}^{-2}).

2.1.4 Anode preparation on carbon cloth

10mg of IrO_2 and 20mg of Vulcan XC-72 were dispersed ultrasonically for 60 minutes in mixture of 1.5 mg 2-propanol and 0.5g of water, together with 85mg of a 5 wt% nafion oligomer solution in lower aliphatic alcohols. The uniform ink obtained was brush-painted by subsequent 7-9 depositions-drying cycles on a 37x30mm carbon cloth (GPP050M from Cetech Co. ltd) previously cleaned ultrasonically and tape-masked to expose an area of 4.3 cm^2 (figure S3). The IrO_2 loading (approx. 1.8 mg cm^{-2}) was estimated by weight difference.

2.1.5 Au-C cathode preparation on carbon cloth

45.2 mg of Au/C 10% electrocatalyst were dispersed ultrasonically for 60 minutes in mixture of 2.0 mg 2-propanol and 1.0 g of water, together with 96 mg of a 5 wt% nafion oligomer solution in lower aliphatic alcohols. The uniform ink obtained was brush-painted by subsequent 5-6 depositions-drying cycles on a 37x30mm carbon cloth (GPP050M from Cetech Co. ltd) previously cleaned ultrasonically and tape-masked to expose an area of 4.3 cm^2 (see scheme S2) until the maximum possible loading on the surface was achieved. The Au/C loading (approx. 0.81 mg_{cat} cm_{geom}^{-2}, 0.081 mg_{Au} cm_{geom}^{-2}) was estimated by weight difference.

2.2 Electrochemical reactor experiments

Experiments were conducted in a 3d-printed ABS gas diffusion flow reactor (figure S2, S4) equipped with two flow buffer layers (cathode and anode) with a circulating 0.2M $KHCO_3$ (Sigma Pure PA) solution on both compartments. Both the liquid and the gases were fed by using a Gilson peristaltic pump equipped with Tygon™ tubes. The cell, vertically oriented, housed in a CO_2-filled drybox, has four compartments: starting from cathode side, i) a gas compartment where pure CO_2 (99.995% purity) was fed; the gas diffusion electrode modified with fac-Mn(apbpy)$(CO)_3$Br complex was housed at the interface between the gas compartment and the cathode buffer layer; the

gas tightness was ensured by two silicon rubber rectangular gaskets with the additional purpose of masking the active area (23 x 18 mm, 4.3 cm^2 exposed surface, (figure S3); ii) and iii) cathodic and anodic buffer layers that were separated by a Nafion 117 membrane; and iv) the anode gas compartment, continuously purged with nitrogen. The anode buffer layer and the anode gas compartment were separated by the carbon cloth GDL modified with IrO_2 water oxidation reaction electrocatalyst. The cathode buffer layer houses also the reference electrode ($Ag|AgCl|KCl_{sat}$) which is closely placed to the cathode electrocatalyst in order to minimize the uncompensated resistance. The buffer layers were filled with circulating 0.2M Bioultra™ $KHCO_3$, (pre-saturated with CO_2 for 30 minutes to remove dissolved oxygen) and high purity (99.995%) CO_2 was fed instead to the cathode gas compartment. The anode gas compartment was continuously evacuated with nitrogen to minimize detrimental oxygen contaminations. The cathode exhaust was fed to the cathode buffer layer tank for gas-liquid separation and pressure equilibration to avoid gas bubbling through the gas diffusion layer. The buffer layer solutions were continuously recycled; the cathode exhaust was sent to and hydraulic guard and vented. Gas was sampled directly in the cathodic cell compartment with a 200ul Hamilton™ gastight syringe through a GC-grade silicon rubber port. The flow rate was 0.2 and 0.4 mL min^{-1} for buffer layers and CO_2 cathode fed respectively. The gas flow rate was traded off to ensure an excess of CO_2 at the cathode without excessively diluting the gas sample. The cathode potential was controlled by setting it to values referenced to the internal reference electrode, while the total cell potential was measured by an external voltmeter. The current collectors were made of stainless steel in a control-sense double connector configuration (figure S2) to minimize the contact IR_{drop}. The solution was not allowed to come in contact with the steel to avoid Fe ions contamination inside the cell. The potential was constantly held (between -1.0V to -1.6V vs $Ag|AgCl|KCl_{sat}$) during every experiment and the gas was sampled at regular time intervals after reaching a steady state and analyzed via gas chromatography; the current was integrated to obtain the charge elapsed. Each electrocatalyst assembly was first tested at different potential to

determine the optimal (in terms of FE and productivity) operating point, then constant cathode potential electrolysis experiments up to 16 hours of duration were performed.

2.3 Product analysis

The gas sampled from the cathodic compartment (100ul) was injected into a Shimadzu gas chromatograph using high purity He (99.995%) as carrier and equipped with a Carboxen WCOT Column, designed to separate hydrogen, O_2, N_2, CO, CO_2 and C_1-C_3 gases; the temperature program was a 140°C 9-minute isotherm, followed by a 30 °C/min ramp to 225°C and an additional holding time of 25 minute. Gas calibration was performed prior to the experiments. The liquid products were analyzed with a Shimadzu high performance liquid chromatograph (HPLC) equipped with a 100ul loop, a column specific for light carboxylic acids and alcohols and a refractive index detector; prior to the injection of the sample the 0.2M $KHCO_3$ buffer was suppressed by passing the sample in a cationic exchange resin to replace K^+ with H^+, decomposing the HCO_3^- as CO_2. The standard calibration curve was made in the same conditions ($HCOO^-$ in 0.2M $KHCO_3$) to minimize the matrix effect. The detection limit was below 50uM for $HCOO^-$ in those conditions.

2.4 Pre- and post-experiments microscopy analysis

The pristine and spent electrode morphological and compositional characterization on the electrode surface was carried out using a Tescan GAIA 3 FIB/SEM microscope equipped with an Edax EDS Octane detector. Both Images and EDS compositional characterization were acquired using an impinging beam energy of 15 keV. Element distribution maps were acquired with a collection time of 600s. The spots analyzed are shown in figure S13.

3 Results:

In order to benchmark the performance of the supported organometallic electrocatalyst, a state-of-the-art carbon-supported Au nanoparticle CO-selective electrocatalyst (Au/C, gold 10 wt% on Vulcan XC-72)[15] was also tested in the complete gas-fed cell. The *fac*-Mn(apbpy)$(CO)_3$Br-modified carbon cloth electrodes (*fac*-Mn(apbpy)$(CO)_3$Br/CC) and carbon supported gold nanoparticles (Au-C/CC) were first tested at different cathodic potentials. Each potentiostatic experiment was performed for an appropriate operation time (from 2 hours at -0.37 V to 30' at -0.82 V vs RHE) depending on the cell current. The faradaic efficiency and partial current profiles at different potentials of both *fac*-Mn(apbpy)$(CO)_3$Br/CC and Au-C/CC are reported in Figures S5 and S6 respectively. The best operating cathode potential was chosen that maximizes the CO-partial current density, to trade-off between faradaic efficiency and CO-productivity. The optimal cathode potentials for fac-Mn(apbpy)$(CO)_3$Br/CC and Au-C/CC were -0.67 and -0.57 V (RHE), respectively. Once the best operating point was determined, an extended electrolysis experiment was performed at each potential. Both electrocatalysts began with a CO-faradaic efficiency (FECO) close to 100% (95% Mn, 90% Au-C/CC) (Figure 2).

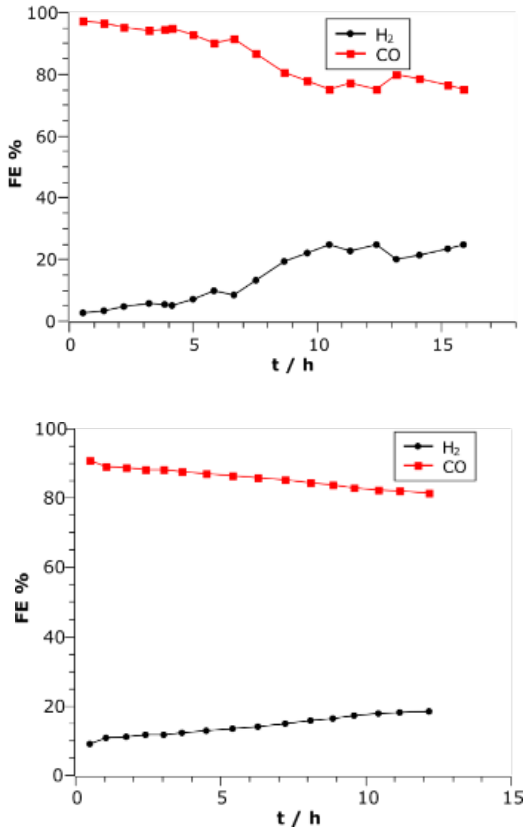

Figure 2: Faradaic efficiency time profile for gaseous products of (top) carbon cloth-supported *fac*-Mn(apbpy)$(CO)_3Br$ ($1.4\cdot10^{-9}$ mol cm_{ECSA}^{-2}, $4.51\cdot10^{-7}$ g_{Mn} cm_{geom}^{-2}) and (bottom) Au/C NPs (0.081 mg_{Au} cm_{geom}^{-2}) operating in buffer layer configuration, CO_2 flow rate 0.2 mL min^{-1}, buffer flow rate 0.4 mL min^{-1}.

The instantaneous cell current and whole cell potential profiles are reported in the SI (figures S7-S10). During the electrolysis, the faradaic efficiency for both electrocatalysts dropped by 25% and 10% for *fac*-Mn(apbpy)$(CO)_3Br$/CC and Au-C/CC respectively (figure 2). The total average current (between each sampling event) for *fac*-Mn(apbpy)$(CO)_3Br$/CC remained almost the same from the beginning to the end, while the CO-partial current shows a decrease accompanied by a steady increase in the H_2-partial current (figure S11), possibly indicating partial electrocatalyst degradation to species promoting HER. The total average current of benchmark Au-C/CC instead showed a

drastic decrease of the total current in the first hour, almost totally driven by the CO-partial current, then a steady decrease at a much slower rate during the rest of the experiment. The H_2-partial current increased only slightly during the experiment, remaining almost constant. Such a performance drop can be ascribed to nanoparticle surface modification during electro-catalysis since no aggregation for this particular Au/C-based material was reported in a comparable time window [15].

Table 1 Relevant electrochemical parameters for electrolysis experiments with *fac*-Mn(apbpy)$(CO)_3$Br/CC and Au/CC NPs.

	fac-Mn(apbpy)$(CO)_3$Br/CC (E = -0.67V)	Au/C NPs (E = -0.57V)
FE_{H2}	13.7%	15.7%
FE_{CO}	76.2%	82.4%
FE_{HCOOH}	10.1%	1.9%
$FE_{totalCO2}$	86.3%	89.0%
$Prod_{CO}$ (Nl min^{-1} g_{Met}^{-1})	69.2	0.318
HCOOH (g min^{-1} $gMet^{-1}$)	16.9	0.0152
TON_{CO}	145286	1999[a]
TON_{HCOOH}	19252	47.4[a]
$TON_{totalCO2}$	164539	2045.97[a]
avg TOF_{CO}	2.54	0.0457
avg TOF_{HCOOH}	0.336	0.00108
avg $TOF_{totalCO2}$	2.87	0.0467

[a] TON and TOF for nanoparticles are considered with respect to the total metal mass present

Table 1 summarizes the relevant electrocatalytic parameters of the constant potential experiments for *fac*-Mn(apbpy)$(CO)_3$Br/CC and Au-C/CC. The metal mass-weight productivity for Au-C/CC electrocatalyst was instead almost three orders of magnitude less, about 0.32 normal-liters of CO min^{-1} per gram of Au (figure S12). The CO_2RR turnover number of *fac*-Mn(apbpy)$(CO)_3$Br/CC

electrocatalyst over 16h of operation was more than $1.6 \cdot 10^5$ ($1.2 \cdot 10^5$ in 12h) compared to Au-C/CC electrocatalyst (calculated on the total gold mass present) that is almost two orders of magnitude less ($2 \cdot 10^3$) (Figure 3).

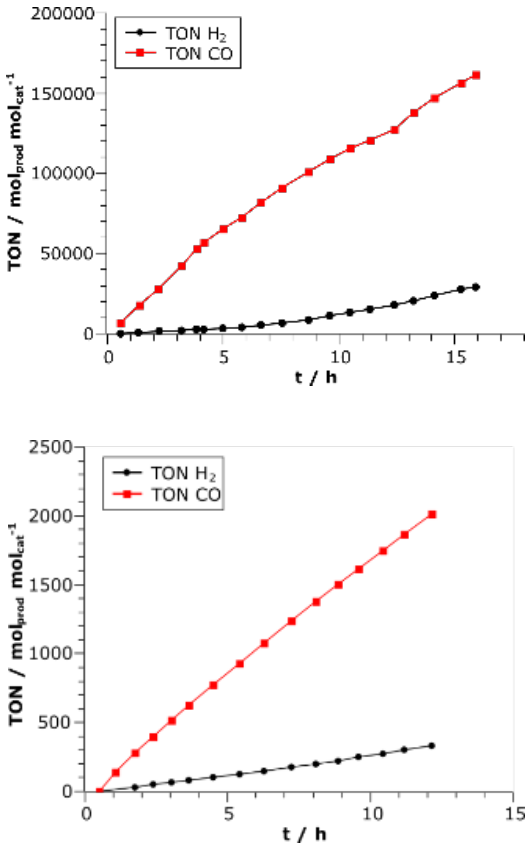

Figure 3: TON time profiles for gaseous products of (top) carbon cloth-supported *fac*-Mn(apbpy)$(CO)_3$Br ($1.4 \cdot 10^{-9}$ mol cm_{ECSA}^{-2}, $4.51 \cdot 10^{-7}$ g_{Mn} cm_{geom}^{-2}) and (bottom) Au/C NPs (0.081 mg_{Au} cm_{geom}^{-2}) operating in buffer layer configuration, CO_2 flow rate 0.2 mL min^{-1}, buffer flow rate 0.4 mL min^{-1}.

In order to investigate the stability of the fac-Mn(apbpy)$(CO)_3$Br/CC electrocatalyst, the pristine and used electrode was scrutinized with SEM microscopy with an EDS dispersive detector to map the distribution of the elements on the electrode surface. The pristine and used electrode micrographs are shown in figure 4. The microanalysis of the pristine electrode (figure 4 and figure S15) shows a uniform distribution of Mn on the electrode surface, with no aggregates present. The

used electrode (figure 4) does not show significant Mn loss phenomena as the Mn surface distribution and density are almost unchanged (table S1 and S2).

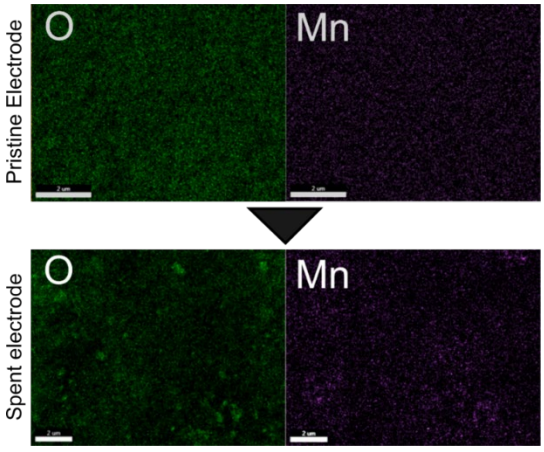

Figure 4: SEM EDAX element mapping of both pristine and used *fac*-Mn(apbpy)$(CO)_3$Br-modified carbon cloth electrode.

4. Discussion:

The *fac*-Mn(apbpy)$(CO)_3$Br electrocatalyst covalently grafted onto a carbon cloth diffusion layer was employed for the first time in a complete gas-fed electrochemical cell. Unlike half-cell systems, this type of configuration of system is potentially scalable by increasing the electrode surface area and stacking multiple cells provided that the performance is not degraded by the conditions. The electrocatalyst operating at the liquid-gas interface showed a TON value almost four times that reported for a half cell (CO_2-saturated electrolyte) study [47] suggesting that the enhanced mass transport due to CO_2 gas-feeding plays an important role in the overall electrocatalytic performance as was already reported for metal nanoparticles [7,28]. Furthermore, the CO average productivity observed for *fac*-Mn(apbpy)$(CO)_3$Br/CC was 70 normal-liters of CO min^{-1} per gram of Mn, more than four times than the half-cell study (14.5 Nl_{CO} min^{-1} g_{Mn}^{-1}). It is noteworthy that the metal loading for *fac*-Mn(apbpy)$(CO)_3$Br/CC (corresponding to a monolayer of anchored complex) is more than two orders of magnitude less than Au/C, with similar CO-partial current performance,

resulting in very high metal efficiency. In fact, the CO-mass specific currents, (8930 A g_{Mn}^{-1}) for the anchored Mn-complex electrocatalyst are much higher than for the Au-C electrocatalyst (41.6 A g_{Au}^{-1}); this further stresses the high metal efficiency of the grafted organometallic complex. A difference in HCOOH-selectivity was observed though when the results are compared to the half-cell study for the *fac*-Mn(apbpy)$(CO)_3$Br/CC. In particular, no formate was detected after 10h of operation at the same cathodic potential in previous the half-cell study [47]. Instead, a FE_{HCOOH} of 10% was observed in the gas-fed system, with a productivity of 16.9 g min^{-1} gMn^{-1} (1.01 kg h^{-1} g_{Mn}^{-1}) (table 1). Such a selectivity difference was also observed by Reisner et al. at different electrocatalyst loadings for [MnBr(2,2′-bipyridine)$(CO)_3$] in aqueous conditions [43]. In particular, at high electrocatalyst loading, the CO-producing pathway was preferred. These observations have been explained considering that at high loading the Mn centers can interact (and dimerize), leading to the production of CO, while at low loading the formation of Mn hydride become feasible, which enhances the formate production [43]. However, in the case of the gas-fed full cell experiments compared to the half-cell experiments, the difference cannot be ascribed to a different loading of the electrocatalyst as the preparation of the electrocatalyst is identical. Also a decrease in the electrocatalyst loading during the experiment can be ruled out, as no significant leaching of the electrocatalyst was observed (Figure 4). Hence the difference in selectivity can be hypothesized to be related to a lower interfacial pH due to the presence of pure CO_2 in the GDL, buffering the pH by consuming OH^- formed both by CO_2RR and HER to produce HCO_3^-. It is reported that more acidic conditions in homogeneous Mn-bpy solutions increase the production of the hydride and hence formate.[22] The higher proton activity (compared to half-cell, buffered only with HCO_3^-) can slightly shift the kinetics to the formation of a hydride that reacts with CO_2 to form HCOOH [43]. This can explain the increased side production of HCOOH in the gas-fed case. Despite this lower CO-selectivity, the two products (CO and HCOOH, as formate) are in different phases (gas and buffer layer respectively), hence their separation is not challenging in a scaled-up electrolysis system.

Regarding the stability, some areas show a higher oxygen density with no apparent correlation with the manganese distribution. This can be related to residual potassium carbonate crystals covering the electrocatalyst surface as a result of contact with the electrolyte: table S2 shows a dramatic increase in the element fraction of both oxygen and potassium compared to the pristine electrode (table S1). Conversely, the formation of manganese hydroxides or carbonates deriving from the decomposition of *fac*-Mn(apbpy)$(CO)_3$Br can be ruled out. In addition, the results of the recorded ATR spectra of the CC after 16 hours electrolysis (Figure S20) it still revealing CO signals (although showing some broadening and decrease in intensity) suggesting the retention of the coordinative structure around manganese after the electrolysis. The decrease of the CO peaks may explain the decreased CO faradaic efficiency in terms of slight decrease of the active sites, considering the very low catalyst surface loading. Furthermore, it should be noted that the limited drop of FE and J_{CO} occurred after $1.6 \cdot 10^5$ CO_2 turnovers in 16hours: so during this time frame the electrocatalyst can be considered stable as metal loading of Mn is two orders of magnitude less than that of gold for Au-C/CC with similar performance and stability. Increasing the electrochemical surface area (by replacing the support material) of the electrode can allow larger metal loadings on a geometric area basis, allowing much longer and higher performance, opening the possibility of scaling up the process to an industrial scale.

5. Conclusions

Concluding, carbon cloth gas diffusion layer-supported *fac*-Mn(apbpy)$(CO)_3$Br organometallic CO_2RR electrocatalyst, operating in a complete gas-fed CO_2 buffer layer electrolyzer, showed a performance almost four times greater in terms of TON, 50% higher in terms of FE, and more than an order of magnitude in terms of volumetric productivity compared to the same material in a half-cell study. The electrode outperforms a benchmark state-of-the-art gold metal nanoparticle on carbon electrocatalyst, despite a metal loading more than two orders of magnitude less. To the best

of our knowledge this is the first example of a covalently bound organometallic complex employed in a complete gas-fed CO_2RR electrolyzer, opening the possibility of scaling up the process to larger scales employing a cost-effective metal-efficient Mn-based electrocatalyst.

Acknowledgements

The Italian Ministry MIUR Italy and Regione Piemonte are kindly acknowledged for financial support through the PRIN 2017 Project (Grant No. 2017YH9MRK) and Saturno Project (Bioeconomy).

References

1 J. Septavaux, C. Tosi, P. Jame, C. Nervi, R. Gobetto and J. Leclaire, Simultaneous CO_2 capture and metal purification from waste streams using triple-level dynamic combinatorial chemistry, Nat. Chem. 12 (2020) 202–212, https://doi.org/10.1038/s41557-019-0388-5.

2 D. U., Hu, X.-M., Pedersen, S. U., Daasbjerg, K., Skrydstrup, T., Scalable carbon dioxide electroreduction coupled to carbonylation chemistry, Nat. Commun., 8 (2017) 489, https://doi.org/10.1038/s41467-017-00559-8.

3 M. E. Boot-Handford, J. C. Abanades, E. J. Anthony, M. J. Blunt, S. Brandani, N. Mac Dowell, J. R. Fernandez, M. C. Ferrari, R. Gross, J. P. Hallett, R. S. Haszeldine, P. Heptonstall, A. Lyngfelt, Z. Makuch, E. Mangano, R. T. J. Porter, M. Pourkashanian, G. T. Rochelle, N. Shah, J. G. Yao and P. S. Fennell, Carbon capture and storage update, Energy Environ. Sci. 7 (2014) 130-189, https://doi.org/10.1039/C3EE42350F.

4 G. Centi, E. A. Quadrelli and S. Perathoner, Catalysis for CO_2 conversion: a key technology for rapid introduction of renewable energy in the value chain of chemical industries, Energy Environ. Sci. 6 (2013) 1711-1731, https://doi.org/10.1039/C3EE00056G.

5 G. Centi and S. Perathoner, Opportunities and prospects in the chemical recycling of carbon dioxide to fuels, Catal. Today 2009, 148 (2009) 191-205, https://doi.org/10.1016/j.cattod.2009.07.075.

6 M. Gattrell and N. Grupta, A. Co, A review of the aqueous electrochemical reduction of CO_2 to hydrocarbons at copper, J. Electroanal. Chem. 594 (2006) 1-19, https://doi.org/10.1016/j.jelechem.2006.05.013.

7 Y. Hori, A. Murata and R. Takahashi, Formation of hydrocarbons in the electrochemical reduction of carbon dioxide at a copper electrode in aqueous solution, J. Chem. Soc. Faraday Trans. 1, 85 (1989) 2309-2326, https://doi.org/10.1039/F19898502309.

8 B. Hu, C. Guild and S. L. Sui, Thermal, electrochemical, and photochemical conversion of CO_2 to fuels and value-added products, J. CO_2 Util. 1 (2013) 18-27, https://doi.org/10.1016/j.jcou.2013.03.004.

9 F. Franco, C. Rettenmaier, H. S. Jeon and B. R. Cuenya, Chem Soc Rev, Transition metal-based catalysts for the electrochemical CO2 reduction: from atoms and molecules to nanostructured materials, 49 (2020) 6884-6946, https://doi.org/10.1039/d0cs00835d.

10 M. Rakowski Dubois and D. L. Dubois, Acc. Chem. Res., Development of Molecular Electrocatalysts for CO_2 Reduction and H_2 Production/Oxidation, 42 (2009) 1974-1982, https://doi.org/10.1021/ar900110c.

11 Q. Lu and F. Jiao, Electrochemical CO_2 reduction: Electrocatalyst, reaction mechanism, and process engineering, Nano Energy 29 (2016) 439-456, https://doi.org/10.1016/j.nanoen.2016.04.009.

12 J. Durst, A. Rudnev, A. Dutta, Y. Fu, J. Herranz, V. Kaliginedi, A. Kuzume, A. A. Permyakova, Y. Paratcha, P. Broekmann and T. J. Schmidt, Electrochemical CO_2 Reduction –

A Critical View on Fundamentals, Materials and Applications, Chimia 69 (2015) 769-776, https://doi.org/10.2533/chimia.2015.769.

13 C. Oloman and H. Li, Electrochemical Processing of Carbon Dioxide, ChemSusChem 1 (2008) 385-391, https://doi.org/10.1002/cssc.200800015.

14 Y. Hori, Modern, Aspects of Electrochemistry, Springer, New York, 2008, Vol.42, Ch. 3.

15 M. Bellini, M. G. Folliero, C. Evangelisti, Q. He, Y. Hu, M. V. Pagliaro, W. Oberhauser, A. Marchionni, J. Filippi, H. A. Miller and F. Vizza, A Gold–Palladium Nanoparticle Alloy Catalyst for CO Production from CO_2 Electroreduction, Energy Technol. 7 (2019) 1800859, https://doi.org/10.1002/ente.201800859.

16 M. Jitaru, D. A. Lowy M. Toma, B. C. Toma and L. ONICIU, Electrochemical reduction of carbon dioxide on flat metallic cathodes, J. Appl. Electrochem. 27 (1997) 875-889, https://doi.org/10.1023/A:1018441316386.

17 Yo. Hori, R. Takahashi, Y. Yoshinami and A. Murata, Electrochemical Reduction of CO at a Copper Electrode, J. Phys. Chem. B 101 (1997) 7075-7081, https://doi.org/10.1021/jp970284i.

18 R. Shiratsuchi and G. Nogami, Pulsed Electroreduction of CO_2 on Silver Electrodes, J. Electrochem. Soc., 143 (1996) 582-586, https://doi.org/10.1149/1.1836484.

19 D. D. Zhu, J. L. Liu and S. Z Qiao, Recent Advances in Inorganic Heterogeneous Electrocatalysts for Reduction of Carbon Dioxide, Adv. Mater. 28 (2016) 3423-3452, https://doi.org/10.1002/adma.201504766.

20 M. Karamad, V. Tripkovic and J. Rossmeisl, Intermetallic Alloys as CO Electroreduction Catalysts—Role of Isolated Active Sites, ACS Catal. 4 (2014) 2268-2273, https://doi.org/10.1021/cs500328c.

21 R. Francke, B. Schille,M and Roemelt, Homogeneously Catalyzed Electroreduction of Carbon Dioxide-Methods, Mechanisms, and Catalysts, Chem. Rev., 118 (2018) 4581-4701, https://doi.org/10.1021/acs.chemrev.7b00459.

22 F. Franco, C. Cometto, L. Nencini, C. Barolo, F. Sordello, C. Minero, J. Fiedler, M. Robert, R. Gobetto and C. Nervi, Local Proton Source in Electrocatalytic CO_2 Reduction with [Mn(bpy–R)$(CO)_3$Br] Complexes, Chem. Eur. J. 23 (2017) 4782-4793, https://doi.org/10.1002/chem.201605546.

23 Franco, C. Cometto, F. F. Vallana, F. Sordello, E. Priola, C. Minero, C. Nervi and R. Gobetto, A local proton source in a [Mn(bpy-R)$(CO)_3$Br]-type redox catalyst enables CO_2 reduction even in the absence of Brønsted acids, Chem. Commun. 50 (2014) 14670-14673, https://doi.org/10.1039/C4CC05563B.

24 J. Hawecker, J.-M. Lehn and R. Ziessel, Electrocatalytic Reduction of Carbon Dioxide Mediated by Re(bipy)(CO)Cl (bipy = 2,2'-bipyridine), J. Chem. Soc. Chem. Commun. (1984) 328-330, https://pubs.rsc.org/en/content/articlepdf/1984/c3/c39840000328.

25 J. M. Smieja and C. P. Kubiak, Re(bipy-tBu)$(CO)_3$Cl−improved Catalytic Activity for Reduction of Carbon Dioxide: IR-Spectroelectrochemical and Mechanistic Studies, Inorg. Chem. 49 (2019) 9283-9289, https://doi.org/10.1021/ic1008363.

26 M. Bourrez, F. Molton, S. Chardon-Noblat and A. Deronzier, [Mn(bipyridyl)$(CO)_3$Br]: An Abundant Metal Carbonyl Complex as Efficient Electrocatalyst for CO_2 Reduction, Angew. Chem., Int. Ed. 50 (2011) 9903-9906, https://doi.org/10.1002/anie.201103616.

27 M. L. Clark, K. A. Grice, C. E. Moore, A. L. Rheingold and C. P. Kubiak, Electrocatalytic CO2 reduction by M(bpy-R)$(CO)_4$ (M = Mo, W; R = H, tBu) complexes. Electrochemical, spectroscopic, and computational studies and comparison with group 7 catalysts, Chem. Sci. 5 (2014) 1894-1900, https://doi.org/10.1039/C3SC53470G.

28 F. Franco, C. Cometto, F. Sordello, C. Minero, L. Nencini, J. Fiedler, R. Gobetto and C. Nervi, Electrochemical Reduction of CO_2 by M$(CO)_4$(diimine) Complexes (M=Mo, W): Catalytic Activity Improved by 2,2′-Dipyridylamine, ChemElectroChem 2 (2015) 1372-1379, https://doi.org/10.1002/celc.201500115.

29 N. Furuya and K. Matsui, Electroreduction of carbon dioxide on gas-diffusion electrodes modified by metal phthalocyanines, J. Electroanal. Chem. 271 (1989) 181-191, https://doi.org/10.1016/0022-0728(89)80074-9.

30 N. Furuya and S. Koide, Electroreduction of carbon dioxide by metal phthalocyanines, Electrochim. Acta 36 (1991) 1309-1313, https://doi.org/10.1016/0013-4686(91)80010-6.

31 P. Kang, S. Zhang, T. J. Meyer, and M. Brookhart, Rapid Selective Electrocatalytic Reduction of Carbon Dioxide to Formate by an Iridium Pincer Catalyst Immobilized on Carbon Nanotube Electrodes, Angew. Chem. Int. Ed. 53 (2014) 8709-8713, https://doi.org/10.1002/anie.201310722.

32 C.M. Lieber and N. S. Lewis, Catalytic reduction of carbon dioxide at carbon electrodes modified with cobalt phthalocyanine, J. Am. Chem. Soc. 106 (1984) 5033-5034, https://doi.org/10.1021/ja00329a082.

33 T. Abe, H. Imaya,T. Yoshida, S. Tokita, D. Schlettwein, D. Ohrle and M. Okaneko, Electrochemical CO_2 Reduction Catalysed by Cobalt Octacyanophthalocyanine and its Mechanism, J. Porphyr. Phthalocyanines, 1 (1997) 315-321, https://doi.org/10.1002/(SICI)1099-1409(199710)1:4%3C315::AID-JPP35%3E3.0.CO;2-V.

34 T. Abe, F. Taguchi, T. Yoshida, S. Tokita, G. Schnurpfeil, D. Wiihrle and M. Kaneko, Electrocatalytic CO_2 reduction by cobalt octabutoxyphthalocyanine coated on graphite electrode, J. Mol. Catal. A Chem 112 (1996) 55-61, https://doi.org/10.1016/1381-1169(96)00242-7.

35 A. Ramos Sende, C. R. Arana, J. L. Hernhndez, K. T. Potts,M. Meshevarz-K and H. D. Abruiia, Electrocatalysis of CO_2 reduction in aqueous media at electrodes modified with electropolymerized films of vinylterpyridine complexes of transition metals, Inorg. Chem. 34 (1995) 3339-3348, https://doi.org/10.1021/ic00116a028.

36 H.-Z. Zhao, Y. Chang and C. Liu, Electrodes modified with iron porphyrin and carbon nanotubes: application to CO_2 reduction and mechanism of synergistic electrocatalysis, J. Solid State Electrochem. 17 (2013) 1657-1664, https://doi.org/10.1007/s10008-013-2027-1.

37 T. Atoguchi, A. Aramata, A. Kazusaka and M. Enyo, Electrocatalytic activity of Co^{II} TPP-pyridine complex modified carbon electrode for CO_2 reduction, J. Electroanal. Chem. 318 (1991) 309–320, https://doi.org/10.1016/0022-0728(91)85312-D.

38 T. V. Magdesieva, T. Yamamoto, D. A. Tryk and A. Fujishima, Electrochemical Reduction of CO_2 with Transition Metal Phthalocyanine and Porphyrin Complexes Supported on Activated Carbon Fibers, J. Electrochem. Soc. 149 (2002) D89-D95, https://doi.org/10.1149/1.1475690.

39 T. Yoshida, K. Kamato, M. Tsukamoto, T. Iida, D. Schlettwein, D. Wöhrle and M. Kaneko, Selective electroacatalysis for CO_2 reduction in the aqueous phase using cobalt phthalocyanine/poly-4-vinylpyridine modified electrodes, J. Electroanal. Chem. 385 (1995) 209-225, https://doi.org/10.1016/0022-0728(94)03762-R.

40 S. Chardon-Noblat, A. Deronzier, R. Ziessel and D. Zsoldos, Electroreduction of CO_2 catalyzed by polymeric $[Ru(bpy)(CO)_2]_n$ films in aqueous media: Parameters influencing the reaction selectivity, J. Electroanal. Chem. 444 (1998) 253-260, https://doi.org/10.1016/S0022-0728(97)00584-6.

41 S. Komatsu, M. Tanaka, A. Okumura and A. Kung, Preparation of cu-solid polymer electrolyte composite electrodes and application to gas-phase electrochemical reduction of CO_2, Electrochim. Acta 40 (1995) 745-753, https://doi.org/10.1016/0013-4686(94)00325-U.

42 N. Morlane´s, K. Takanabe and V. Rodionov, Simultaneous Reduction of CO_2 and Splitting of H_2O by a Single Immobilized Cobalt Phthalocyanine Electrocatalyst, ACS Catal. 6 (2016) 3092-3095, https://doi.org/10.1021/acscatal.6b00543.

43 B. Reuillard, K. H. Ly, T. E. Rosser, M. F. Kuehnel, I. Zebger and E. Reisner, Tuning Product Selectivity for Aqueous CO_2 Reduction with a Mn(bipyridine)-pyrene Catalyst Immobilized on

a Carbon Nanotube Electrode, J. Am. Chem. Soc., 139 (2017) 14425-14435, https://doi.org/10.1021/jacs.7b06269.

44 C. Sun, R. Gobetto and C. Nervi, Recent advances in catalytic CO_2 reduction by organometal complexes anchored on modified electrodes, New J. Chem. 40 (2016) 5656-5661, https://doi.org/10.1039/C5NJ03426D.

45 S. Sato, K. Saita, K. Sekizawa, S. Maeda and T. Morikawa, Low-Energy Electrocatalytic CO_2 Reduction in Water over Mn-Complex Catalyst Electrode Aided by a Nanocarbon Support and K^+ Cations, ACS Catal., 8 (2018) 4452-4458, https://doi.org/10.1021/acscatal.8b01068.

46 C. Sun, L. Rotundo, C. Garino, L. Nencini, S. S. Yoon, R. Gobetto and C. Nervi, Electrochemical CO_2 Reduction at Glassy Carbon Electrodes Functionalized by Mn^I and Re^I Organometallic Complexes, ChemPhysChem 18 (2017) 3219-3229, https://doi.org/10.1002/cphc.201700739.

47 L. Rotundo, J. Filippi, R. Gobetto, H. A. Miller, R. Rocca, C. Nervi and F. Vizza, Electrochemical CO_2 reduction in water at carbon cloth electrodes functionalized with a fac-Mn(apbpy)$(CO)_3$Br complex, Chem. Commun. 55 (2019) 775-777, https://doi.org/10.1039/C8CC08385A.

48 J. T. Gostick, M. W. Fowler, M. D. Pritzker, M. A. Loannidis and L. M. Behra, In-plane and through-plane gas permeability of carbon fiber electrode backing layers, J. Power Sources 162 (2006) 228-238, https://doi.org/10.1016/j.jpowsour.2006.06.096.

49 Y. Nishimura, D. Yoshuda, M. Mizuhata, K. Asaka, K. Oguro and H. Takenaka, Solid polymer electrolyte CO_2 reduction, Energy Convers. Manag. 36 (1995) 620-632, https://doi.org/10.1016/0196-8904(95)00084-Q.

50 J. Wu, P. P. Sharma, B. H. Harris and X.-D. Zhou, Electrochemical reduction of carbon dioxide: IV dependence of the Faradaic efficiency and current density on the microstructure and thickness of tin electrode, J. of Power Sources 258 (2014) 189-194, https://doi.org/10.1016/j.jpowsour.2014.02.014.

51 D. W. Dewulf and J. Bard, The electrochemical reduction of CO_2 to CH_4 and C_2H_4 at Cu/Nafion electrodes (solid polymer electrolyte structures), Catal. Lett. 1 (1998) 73-80, https://doi.org/10.1016/10.1007/BF00765357.

52 R. L. Cook, R. C. MacDuff and A. F. Sammells, Ambient Temperature Gas Phase CO_2 Reduction to Hydrocarbons at Solid Polymer Electrolyte Cells, J. Electrochem. Soc. 135 (1988) 1470-1471, https://doi.org/10.1149/1.2096030.

53 L.M. Aeshala a, S.U. Rahman and A. Verma, Effect of solid polymer electrolyte on electrochemical reduction of CO_2, Sep. Purif. Technol. 94 (2012) 131-137, https://doi.org/10.1016/j.seppur.2011.12.030.

54 L.M. Aeshala, R.G. Uppaluri and A. Verma, Effect of cationic and anionic solid polymer electrolyte on direct electrochemical reduction of gaseous CO_2 to fuel, J. CO_2 Util. 3–4 (2013) 49-55, https://doi.org/10.1016/j.jcou.2013.09.004.

55 L. M. Aeshala, R. Uppaluri and A. Verma, Electrochemical conversion of CO_2 to fuels: tuning of the reaction zone using suitable functional groups in a solid polymer electrolyte, Phys.Chem.Chem.Phys. 16 (2014) 17588-17594, https://doi.org/10.1039/C4CP02389G.

56 L. Ma, S. Fan, D. Zhen, X. Wu, S. Liu, J. Lin, S. Huang, W. Chen and G. He, Electrochemical Reduction of CO_2 in Proton Exchange Membrane Reactor: The Function of Buffer Layer, Ind. Eng. Chem. Res. 56, (2017) 10242-10250, https://doi.org/10.1021/acs.iecr.7b00819.

57 J. Wu, F. G. Risalvato, P. P. Sharma, P. J. Pellechia, F.-S. Ke and X.-D. Zhou, Electrochemical Reduction of Carbon Dioxide: II. Design, Assembly, and Performance of Low Temperature Full Electrochemical Cells, J. Electrochem. Soc. 160 (2013) F953-F957, https://doi.org/10.1149/2.030309jes.

58 J. Wu, F. G. Risalvato, S. Ma and X.-D. Zhou, Electrochemical reduction of carbon dioxide III. The role of oxide layer thickness on the performance of Sn electrode in a full electrochemical cell, Mater. Chem. A 2, (2014) 1647-1651, https://doi.org/10.1039/C3TA13544F.

59 C. Delacourt, P. L. Ridgway, J. B. Kerr and J. Newman, Design of an Electrochemical Cell Making Syngas ($CO + H_2$) from CO_2 and H_2O Reduction at Room Temperature, J. Electrochem. Soc. 155 (2008) B42-B49, https://doi.org/10.1149/1.2801871.

60 H. Li, C. Oloman, The electro-reduction of carbon dioxide in a continuous reactor, J. Appl. Electrochem. 35 (2005) 955, https://doi.org/10.1007/s10800-005-7173-4.

61 H. Li and C. Oloman, Development of a continuous reactor for the electro-reduction of carbon dioxide to formate–Part 1: Process variables, J. Appl. Electrochem. 36 (2006) 1105, https://doi.org/10.1007/s10800-006-9194-z.

62 H. Li and C. Oloman, Development of a continuous reactor for the electro-reduction of carbon dioxide to formate–Part 2: Scale-up, J. Appl. Electrochem. 37 (2007) 1107-1117, https://doi.org/10.1007/s10800-007-9371-8.

63 E. J. Dufek, T. E. Lister and M. E. McIlwain, Bench-scale electrochemical system for generation of CO and syn-gas, J. Appl. Electrochem. 41 (2011) 623-631, https://doi.org/10.1007/s10800-011-0271-6.

64 J. J. Kaczur, H. Yang, S. Dawar Sajjad and R. I. Masel, US2017/0037522A1.

65 M. Sandroni, G.Volpi, J. Fiedler, R. Buscaino, G. Viscardi, L. Milone, R. Gobetto, C. Nervi, Iridium and ruthenium complexes covalently bonded to carbon surfaces by means of electrochemical oxidation of aromatic amines, Cat. Today 158 (2010) 22–28, https://doi.org/10.1016/j.cattod.2010.06.025.